IEEE Access
Multidisciplinary | Rapid Review | Open Access Journal

Received 7 September 2022, accepted 12 October 2022, date of publication 25 October 2022, date of current version 4 November 2022.

Digital Object Identifier 10.1109/ACCESS.2022.3216707

RESEARCH ARTICLE

Low-Loss Ultrasound Transmission Through Waveguide From Double Parabolic Reflectors (DPLUS) for Thermal Ablation

KANG CHEN[1], TAKASUKE IRIE[2], (Member, IEEE), TAKASHI IIJIMA[3], SUSUMU MIYAKE[1], AND TAKESHI MORITA[1,4], (Member, IEEE)

[1]Graduate School of Frontier Sciences, The University of Tokyo, Chiba 277-8561, Japan
[2]Microsonic Company Ltd., Tokyo 185-0012, Japan
[3]National Institute of Advanced Industrial Science and Technology (AIST), Onogawa, Tsukuba, Ibaraki 305-8569, Japan
[4]Graduate School of Engineering, The University of Tokyo, Bunkyo, Tokyo 113-8656, Japan

Corresponding author: Kang Chen (kchen@s.h.k.u-tokyo.ac.jp)

This work was supported by the JSPS KAKENHI under Grant 20H02097 and Grant 21KK0065. The work of Kang Chen was supported by JSPS DC2 Program (Japan Society for the Promotion of Science Program for Doctoral Course Students) under Grant 21J1082.

ABSTRACT In this paper, to advance acoustic waveguide transducers towards practical thermal ablation applications, we studied DPLUS (double parabolic reflectors wave-guided ultrasonic transducer) with a 1-m long (0.6-mm radius) and low-loss fused quartz thin waveguide working at the optimal frequency of 2.2 MHz, and the thermal effects to the tissue under different ultrasound exposure time. The measured vibration attenuation coefficient of the fused quartz thin waveguide is ∼0.0123 dB/MHz/cm, and such low-loss characteristic is one of the keys of the studied DPLUS for realizing thermal ablation. Under the transmitted axial vibration velocity amplitude v_{max} at the thin waveguide tip of 1 m/s and the ultrasound exposure time of 1 s, 5 s, 10 s, 20 s, the measured temperature rises in the chicken breast tissue showed good agreements with the simulation results. Lesions were observed in the tissue under the exposure of 10 s, 20 s, and 30 s. The lesion size increases with the exposure time but the measured axial and lateral widths of the lesions were smaller than 2 mm. The presented results in this paper showed that thermal ablation was achieved by a m-range long thin-waveguide DPLUS which becomes an important progress of DPLUS towards practical MIT applications.

INDEX TERMS Thermal ablation, DPLUS, waveguide, fused quartz.

I. INTRODUCTION

For biomedical applications, ultrasonic transducers with long waveguides had been used for low-frequency (20-100 kHz) ultrasound angioplasty, minimally invasive thermal treatments (MIT, 1-10 MHz), and microscope (>100 MHz), etc. For treating arterial diseases using low-frequency (20-100 kHz) ultrasound angioplasty, the ultrasonic device mainly includes a high-power Langevin transducer and a meter-long thin waveguide (∼1 mm in diameter, usually made of Nitinol) [1], [2]. Commonly, the thin waveguide length is designed for making the odd-number harmonic resonant frequency of the thin waveguide close to the resonant frequency of the Langevin transducer [3]. By connecting the almost fixed end of the thin waveguide to the Langevin transducer, the vibration displacement in the thin waveguide may be amplified compared with the vibration in the Langevin transducer (with the amplification depending on the stress at the connection part of the thin waveguide and the maximum stress in the thin waveguide) [3], [4]. By resonant excitation, over 100 μm of displacement amplitude at the thin waveguide tip can be realized, which may induce cavitation, non-linear wave propagation, and acoustic streaming in the diseased tissue. The diseased tissue can be destructed mechanically. For microscope (>100 MHz) applications, the ultrasonic device mainly includes a high-frequency ultrasonic

The associate editor coordinating the review of this manuscript and approving it for publication was Riccardo Carotenuto.

transducer (>100 MHz) and a tapered waveguide. Due to the high-frequency ultrasound propagation in the waveguide, the waveguide must be designed with low loss and large signal-to-noise ratio. Amorphous material such as fused quartz is commonly used [5], [6]. One of the ambitions of the waveguide-based microscopes is replacing biopsy [7], [8]: by inserting the thin waveguide, microscopic images of the target can be obtained without taking the tissue sample out of the treatment body, and the diseased tissue can possibly be observed from the microscopic image. Towards this objective, there are currently two problems regarding the design of the waveguide: the first is the low output acoustic power and the second is the low imaging resolution. Designing a focusing mechanism at the waveguide tip can improve the imaging resolution [8] but improving the output acoustic power may require a novel waveguide design since we need to increase the coupling area between the waveguide and transducer for introducing more input power and meanwhile focusing the incident ultrasound.

For minimally invasive thermal treatments (MIT, 1-10 MHz), the ultrasonic device mainly includes a MHz transducer and a tapered thin waveguide, and such device is usually called acoustic waveguide (AW) applicator. AW applicators are attractive mainly for the following reasons. First, unlike interstitial and intracavitary applicators where the piezoelectric element (usually PZT, lead-zirconate-titanite) must be placed near the tumor, the PZT is not inserted to the treatment location for AW applicators and therefore the size of PZT can be made large which results in higher input power to the waveguide. The outer diameters of the PZT tubes used for interstitial and intracavitary applicators are usually smaller than ~4 mm and ~10 mm [9], respectively, however, outer diameter of the PZT disc can be ~40 mm for AW applicators [10]. Higher acoustic output can be potentially realized by AW applicators which would reduce the treatment time and increase the lesion size. Second, unlike interstitial and intracavitary applicators, the resonant frequency control system, power-delivery system, and water-cooling system can be implemented easier for AW applicators since their components are not required to be inserted to the treatment location. Despite the above advantages, the existing AW applicators had not been used for thermal ablation due to the low acoustic output ($\ll 1\,kW/cm^2$) [10], [11], [12]. Although large-size PZT can be used, the current AW applicators lack a revolutionary waveguide design for focusing the incident ultrasound emitted from the large-size PZT. Tapered structures used in current waveguides have not been reported for having a large vibration amplitude amplification (<10 times) [5], [7], [10], [11], [12], [13], [14], nor do they generate appropriate excitation source for exciting the propagation modes in the thin waveguide.

In this paper, we studied a novel transducer called Double Parabolic refLectors wave-guided Ultrasonic tranSducer (DPLUS) and investigated the thermal ablation by DPLUS with a 0.6-mm radius and 1-m long fused quartz thin waveguide. DPLUS can solve the problems of current AW applicators, for example, high acoustic output (>1 kW/cm^2) can be realized due to the large input-energy surface area to the waveguide and the parabolic focusing mechanism introduced by the unique double-parabolic-reflectors design [15]. Such improvement in the acoustic output is a key step towards thermal ablation applications. Future developments of DPLUS (such as high-frequency DPLUS for microscope) might also benefit other applications such as ultrasound angioplasty and microscope.

II. PROPOSED DOUBLE PARABOLIC REFLECTORS WAVE-GUIDED HIGH-POWER ULTRASONIC TRANSDUCER (DPLUS)

A. DPLUS WITH A LONG FUSED QUARTZ THIN WAVEGUIDE

DPLUS structure proposed by us has two parabolic reflectors as illustrated in Fig. 1(a). The first parabolic reflector is for focusing the plane-wavefront ultrasound generated by the PZT ring, and the 2nd parabolic reflector is for turning the focused ultrasound to a plane-wavefront and high-intensity ultrasound. The resultant plane-wavefront wave is effective for exciting the low-frequency propagation mode in the thin waveguide, and therefore the 2nd parabolic reflector is necessary. The amplification of the vibration velocity by two parabolic reflections reaches ~10 times at ~1-2 MHz [15].

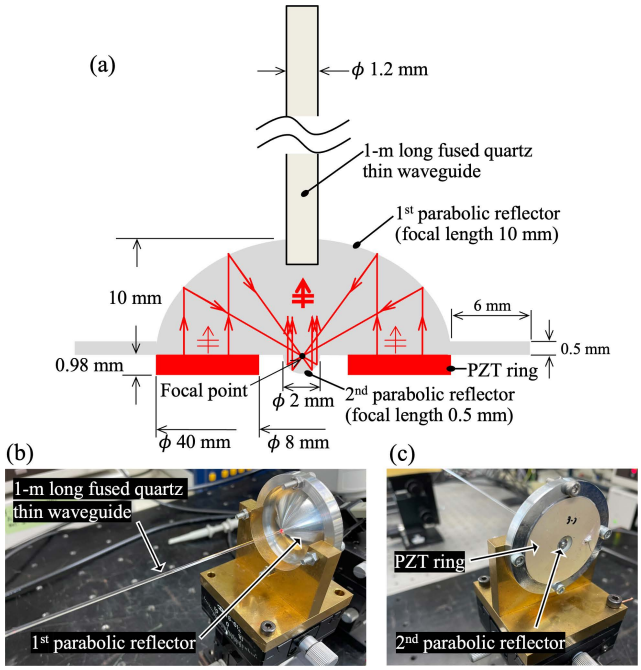

FIGURE 1. DPLUS. (a) Illustration of DPLUS. (b)-(c) An assembled DPLUS prototype.

We had studied DPLUS with ~40 mm long thin waveguide (made of duralumin A2017) in order for understanding the working principle and exploring the excitable vibration amplitude in the thin waveguide [15], [16], [17]. Results showed that ~7 m/s of vibration velocity amplitude could be realized in the thin waveguide and acoustic pressure in

water of over 7 MPa (spatial peak temporal average intensity of ∼1.6 kW/cm^2) between 1 to 2 MHz could be estimated under the resonant excitation of the thin waveguide [15], thus indicating the high-power performance of DPLUS. For MIT applications, we studied DPLUS with a 1-m long Nitinol thin waveguide [18], which revealed that the vibration attenuation in the thin waveguide is one of the most important material indexes for improving the vibration amplitude of the propagated wave. Therefore, low-loss thin waveguide material is required. In our latest work [19], amorphous fused quartz (with the radius of 0.6 mm and length of 40 mm) was selected as the thin waveguide due to its low loss. The innovative points of this paper are twofold: the development of DPLUS with a 1-m long and low-loss fused quartz thin waveguide; the study of thermal ablation effects to the tissue under different ultrasound exposure time. Previous generations of DPLUS had either high-attenuation thin waveguides (such as Nitinol or duralumin A2017) or short thin waveguides (such as 40 mm long), therefore it is the first time for developing DPLUS with a 1-m long and low-loss thin waveguide. For practical applications, 1-m long thin waveguide is necessary. For the 1-m long thin waveguide, the vibration attenuation in the thin waveguide has to be considered, and therefore new modeling results are presented in this paper. This work is an important step towards practical MIT applications.

The assembled DPLUS prototype is shown in Figs. 1(b)-(c). In the current design, the focal length of the 1st and 2nd parabolic reflectors is 10 mm and 0.5 mm, respectively. Two reflectors share the same focal point as shown in Fig. 1(a). The parabolic-reflectors structure was made of duralumin A2017 due to its low-loss, high strength, and good machinability. A hard-type PZT (PZT 18K, NGK Spark Plug Co., Ltd., Nagoya, Japan) was selected which has the inner and outer diameters of ϕ8mm and ϕ40mm, and mechanical quality factor of 1800. As will be revealed in Section III, the optimal frequency for inducing thermal effects to the tissue is 2.15 MHz for a 0.6-mm radius thin waveguide. The thickness (0.98 mm) of the PZT ring was designed for matching the fundamental thickness mode resonant frequency to this optimal frequency. The PZT ring was polarized in the thickness direction with the electrodes covered on the top and bottom surfaces. The fused quartz thin waveguide (Microsonic Co., Ltd., Tokyo, Japan) has a radius of 0.6 mm and a length of 1 m. Both the PZT ring and the fused quartz thin waveguide were glued to the parabolic-reflectors structure using a thermosetting epoxy (EpiFine, Fine Polymers Corporation, Chiba, Japan).

B. CONCEPT OF DPLUS FOR MIT APPLICATIONS

A concept of DPLUS for MIT applications is illustrated in Fig. 2. First, an endoscope is inserted to the treatment location. Then, the DPLUS thin waveguide is inserted through the endoscope. The thin waveguide needs to be protected by a plastic catheter with air in between for avoiding the energy leak to the healthy tissue. The camera on the endoscope can be used for locating the thin waveguide tip to the diseased tissue.

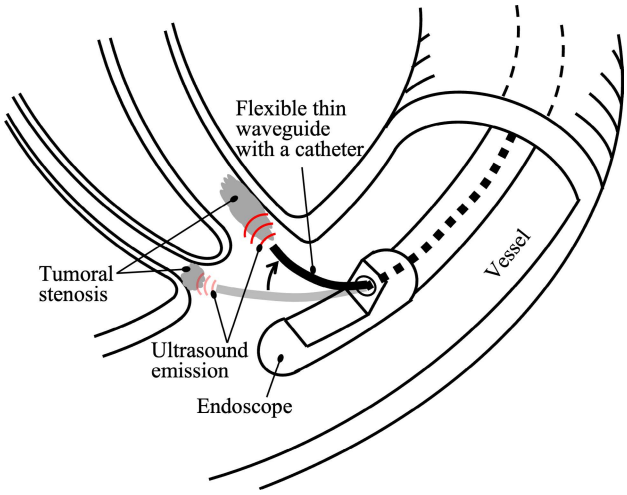

FIGURE 2. A concept of DPLUS for MIT applications.

The movement of the thin waveguide is controlled by pulling and twisting, or by active method such as magnetic field control [20]. After positioning the thin waveguide, ultrasound is delivered through the thin waveguide. The emission of ultrasound can be from the tip of the thin waveguide [19] or along the side surface [10], [11], [18], depending on the design of the thin waveguide. The treatment area can be monitored by the same camera on the endoscope or in real time by magnetic resonance imaging (MRI). With high intensity ultrasound delivered, the target tumor cell is killed almost immediately through coagulative necrosis, without damaging the surrounding healthy tissue. Eventually, the dead cell can be eliminated by the immune process of the treatment body.

III. MODELING OF DPLUS

Theoretical modeling of DPLUS with a 1-m long fused quartz thin waveguide is presented in this section for establishing the relation between the vibration attenuation in the thin waveguide and the optimal working frequency for inducing the thermal effects to the tissue. After double parabolic reflections, the high-intensity plane-wavefront wave is propagated towards the thin waveguide, which further experiences attenuation in the thin waveguide due to the material damping. When propagated at the waveguide-tissue interface, ultrasound reflection and transmission occur due to the acoustic impedance mismatch. The transmitted ultrasound to the tissue induces temperature rise by means of ultrasound absorption. Under sufficient thermal dose, tissue ablation may occur. In order to study these physics, the modeling was divided into five parts: wave propagation in the thin waveguide, ultrasound reflection and transmission, acoustic field in the tissue, ultrasound power deposition, and temperature distribution in the tissue. The modeling methods for the acoustic and temperature fields are the same as our earlier work [19], the main contribution from this work is the consideration of vibration attenuation in the thin waveguide and the ultrasound reflection and transmission at the waveguide-tissue interface.

Therefore, the following mainly describes the modelling of interface axial vibration velocity.

A. A PROPOSED THEORETICAL MODEL OF DPLUS

Figure 3(a) shows the proposed model of DPLUS with a long thin waveguide for thermal treatments. In this theoretical model, we assume that continuous wave is propagated through the thin waveguide, but structure resonance is not excited in the thin waveguide and tissue. The thin waveguide has a length of L and vibration amplitude attenuation coefficient of α_{tw} (in dB/MHz/cm). The incident axial vibration velocity at the left side of the thin waveguide from $r = 0$ to $r = a$ is denoted as v_{in}, which has certain vibration shape according to the propagation modes in the thin waveguide. The maximum value of the incident axial vibration velocity v_{in} along the radial direction (from $r = 0$ to $r = a$) is denoted as incident vibration velocity amplitude $v_{\text{in-max}}$, which was modeled as a constant as illustrated in Fig. 3(b). This constant was set as 0.875 m/s (which can be arbitrary). After propagating a distance of L, the incident axial vibration velocity v_{in} attenuates, and the attenuated axial vibration velocity is denoted as v_{at} which has the same vibration shape as v_{in}. At the contact interface between the tissue and thin waveguide, ultrasound experiences reflection and transmission. The transmitted axial vibration velocity right after but infinitely close to the contact interface from $r = 0$ to $r = a$ is denoted as v, which was assumed having the same vibration shape as v_{in} and v_{at}. The maximum value of the transmitted axial vibration velocity v along the radial direction (from $r = 0$ to $r = a$) is denoted as transmitted axial vibration velocity amplitude v_{max}. By changing the working frequency f and the thin waveguide attenuation coefficient α_{tw}, the axial vibration shape and the vibration attenuation of the propagated wave in the thin waveguide change, which further influences the transmitted axial vibration velocity v, the acoustic intensity field, the deposited ultrasound power, and the temperature distribution in the tissue. The relation between α_{tw}, f, and the temperature field T can be established from this modeling.

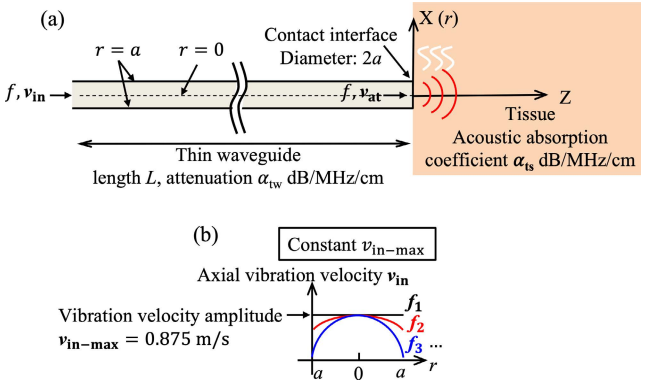

FIGURE 3. Theoretical model. (a) A proposed model of DPLUS with a long thin waveguide. (b) The incident axial vibration velocity v_{in} model.

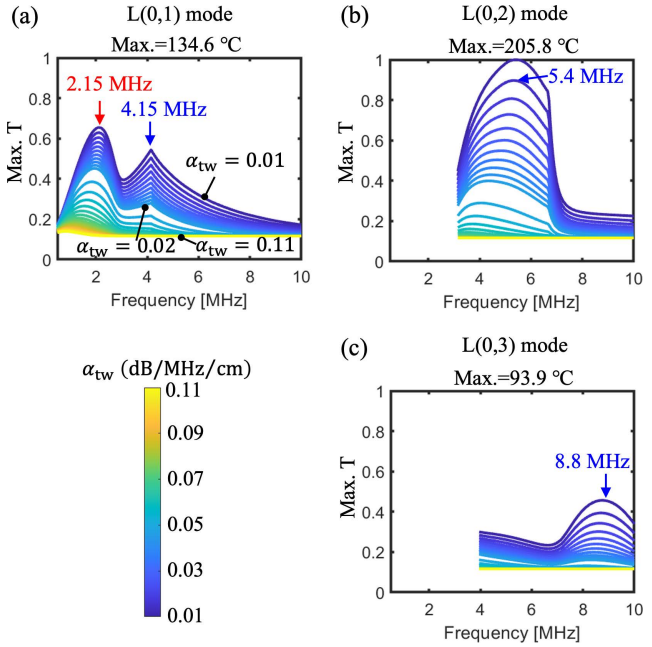

FIGURE 4. Modeling results for (a) L(0,1) mode, (b) L(0,2) mode, and (c) L(0,3) mode. The maximum steady-state temperature was normalized to 205.8 °C. α_{tw} changes from 0.01 to 0.02 dB/MHz/cm with a step of 0.001 dB/MHz/cm, and from 0.025 to 0.11 dB/MHz/cm with a step of 0.005 dB/MHz/cm.

B. WAVE PROPAGATION IN THE THIN WAVEGUIDE

Material damping and wave dispersion are two possible mechanisms for the vibration attenuation in the thin waveguide. If a narrow-band ultrasound is propagated through the thin waveguide as is the case in this modeling, the effect from the wave dispersion can be ignored. Considering only the material damping effect, the axial vibration velocities v_{in} and v_{at} can be modelled by:

$$v_{\text{at}} = v_{\text{in}} \times 10^{(-\alpha_{\text{tw}} f L/20)}, \tag{1}$$

where f is the ultrasound frequency in MHz, α_{tw} is vibration attenuation coefficient in dB/MHz/cm, L is the thin waveguide length in cm. We assume that the ultrasound attenuation $\alpha_{\text{tw}} \times f$ has a linear relation with f. In this modeling, L is 100 cm, α_{tw} has a variation from 0.01 to 0.11 dB/MHz/cm, and f is from 0.5 to 10 MHz.

The transmitted axial vibration velocity v right after the contact interface between the tissue and thin waveguide was calculated as:

$$v = \left| \frac{2Z_{\text{ac}}}{Z_{\text{rd}} + Z_{\text{ac}}} \right| v_{\text{at}}, \tag{2}$$

where v_{at} is the attenuated axial vibration velocity described by Eq. (1), Z_{ac} is the acoustic impedance of the propagation mode in the thin waveguide and equals to $\rho c_{\text{p}}/S$, ρ is the material density of the thin waveguide, c_{p} is the phase velocity, S is the cross-section area of the thin waveguide, and Z_{rd} is the radiation impedance from the thin waveguide to the tissue [21].

The vibration shape of v (or v_{in} or v_{at}) was calculated by the Pochhammer-Chree wave theory [22] described in the Supplementary Note 1 of the supplementary material. In addition, the acoustic and temperature distributions (solved by the bio-heat transfer equation (BHTE) [23] and Finite-Difference Method (FDM) [24]) in the tissue were detailly described in the Supplementary Note 2 of the supplementary material. The calculation mode for the temperature rises in the tissue can be referred to Fig. 5 of our latest work [19], and some important points are also summarized in Supplementary Note 3 of the supplementary material. The tissue material properties for common soft tissues are shown in TABLE 1.

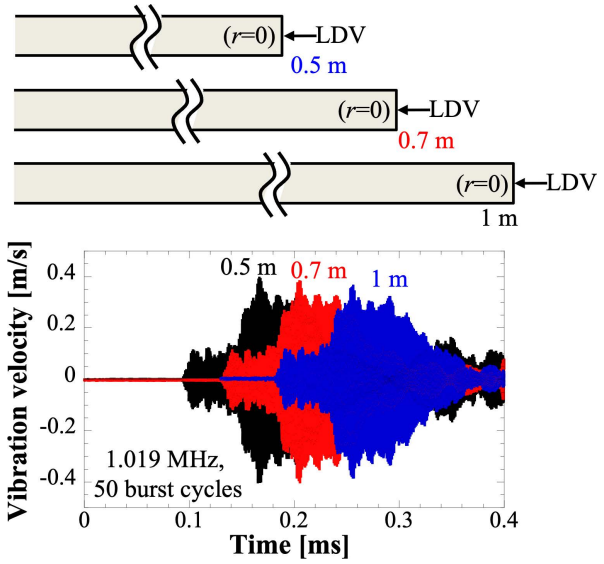

FIGURE 5. Vibration attenuation measurement of the fused quartz thin waveguide at 1.019 MHz.

TABLE 1. Material properties for the temperature distribution calculation.

	Thin waveguide (Fused quartz)	Tissue
Density (kg/m^3)	2203	1000
Poisson ratio	0.17	/
Sound velocity c_d (m/s)	5914	1500
Thermal conductivity κ (W/m/°C)	1.38	0.5
Thermal diffusivity α (m^2/s)	0.93×10^{-6}	0.15×10^{-6}
Tissue absorption coefficient α_{ts} (dB/MHz/cm)	/	0.5
Heat convection coefficient of air h_{air} (W/m^2/°C)	25	
Element mesh size $dx = dz$ (μm)	50	
Atmosphere temperature T_{atmos} (°C)	24	

C. MODELING RESULTS

For describing the induced thermal effects to the tissue, the maximum steady-state temperature in the tissue (denoted as Max. T) was representatively chosen. It is considered that a higher steady-state temperature represents a better thermal effect to the tissue. Under the thin waveguide radius a of 0.6 mm, the maximum steady-state temperature in the tissue for the first three modes under different values of frequency f and attenuation coefficient α_{tw} are shown in Fig. 4. α_{tw} changes from 0.01 to 0.02 dB/MHz/cm with a step of 0.001 dB/MHz/cm, and from 0.025 to 0.11 dB/MHz/cm with a step of 0.005 dB/MHz/cm. The cut-off frequencies are 3.1 MHz and 3.79 MHz for the L(0,2) and L(0,3) modes, and beyond which these modes can be excited. For the L(0,1) mode, it can be excited at any frequency. As shown in Fig. 4, the optimal frequency depends on α_{tw} and the propagation mode. When the attenuation coefficient $\alpha_{tw} \leq \sim$0.02 dB/MHz/cm, the optimal frequencies almost have no change under different α_{tw}, which are 2.2 MHz and 4.15 MHz for the L(0,1) mode, 5.4 MHz for the L(0,2) mode, and 8.8 MHz for the L(0,3) mode as labeled in Fig. 4. When the attenuation coefficient $\alpha_{tw} > \sim$0.02 dB/MHz/cm, the optimal frequency for the L(0,1) mode tends to be at a lower frequency, and large steady-state temperature is difficult to be realized at high frequencies for the L(0,2) and L(0,3) modes. Under large α_{tw} and ultrasound frequency, the ultrasound energy is mainly dissipated in the thin waveguide due to material damping. As will be shown in the subsection *A. Measurement of the vibration attenuation in the thin waveguide* of Section IV, the measured attenuation coefficient α_{tw} of fused quartz thin waveguide is close to 0.01 dB/MHz/cm, and therefore we will focus on the curves with α_{tw} of 0.01 dB/MHz/cm in Fig. 4. From the modeling results, the best thermal effect can be expected from the L(0,2) mode at 5.4 MHz.

To use high frequencies such as 5.4 MHz, two following points must be considered. (1) Multi-mode excitation. When the excitation frequency (such as 5.4 MHz) is larger than the cut-off frequencies, multiple propagation modes might be excited in the thin waveguide. Care must be taken for considering the contribution to the tissue thermal effect from each propagation mode. (2) Achievable vibration velocity amplitude. Considering multi-mode excitation, each propagation mode has certain vibration amplitude and takes certain energy from the excitation source. Therefore, to obtain enough vibration amplitude for a specific mode becomes difficult. Considering these, the L(0,2) mode at 5.4 MHz is not an optimal choice.

The L(0,1) mode at an optimal frequency of 2.15 MHz becomes the best choice for the following reasons. (1) Excitable vibration velocity amplitude. Below 3 MHz, our experimental results showed that ~3 m/s peak value of the axial vibration velocity at the thin waveguide tip could be measured [19], which is large enough for realizing thermal ablation. Such high vibration velocity amplitude at high frequencies >4 MHz has not been experimentally obtained. (2) Easy excitation of the mode. At 2.15 MHz, only the L(0,1) propagation mode can be excited. (3) Optimal thermal effect. 2.15 MHz is the optimal frequency for the L(0,1) mode, showing the highest steady-state temperature value.

For the modeling results in Fig. 4, we fixed the thin waveguide radius a to 0.6 mm based on the available radius of the fused quartz fiber purchased from Microsonic Co., Ltd. (Tokyo, Japan). By using the attenuation coefficient α_{tw} of 0.01 dB/MHz/cm, the modeling results by changing the radius a from 0.1 mm to 2 mm showed almost the same optimal a/Λ where a is the thin waveguide radius and $\Lambda = c_p/f$ is the wavelength in the thin waveguide. Same a/Λ means the same axial vibration velocity shape in the thin waveguide. Larger thin waveguide diameter is needed for increasing the contact area to the tissue and thus potentially increasing the treatment area, so the radius of 0.6 mm was chosen.

The presented optimal frequency (2.15 MHz) for α_{tw} of 0.01 dB/MHz/cm is also effective for a variation of tissue material properties (with the acoustic absorption coefficient α_{ts} changing from 0.1 to 2 dB/MHz/cm, and the frequency dependence of the absorption term $\alpha_{ts} \times f^{\beta}$ changing from $\beta = 1$ to $\beta = 1.18$). This means that the modeling results can be applied to common soft tissue. In addition, the vibration amplitude attenuation coefficient α_{tw} in the thin waveguide might have certain frequency dependence, for example, for common crystalline metals such as duralumin, brass, steel, the ultrasound attenuation (α in dB/cm) mainly depends on the microstructural grain and temperature, which can be written as $\alpha = \alpha_{tw} \times f^1$ (linear to the frequency) for longitudinal (dilatational) waves below ~5 MHz at the room temperature [25]. For amorphous fused quartz, it might be reasonable to approximate the attenuation as $\alpha = \alpha_{tw} \times f^1$ below 10 MHz. This means that the modeling method for the vibration attenuation in the thin waveguide might also be effective.

IV. MEASUREMENT RESULTS AND DISCUSSIONS

Under the optimal design of the thin waveguide, a DPLUS prototype working at 2.2 MHz with a 0.6-mm radius and 1-m long fused quartz thin waveguide was fabricated. Modeling results showed less than 1% difference in the maximum steady-state temperature between 2.15 MHz and 2.2 MHz, and therefore 2.2 MHz can be approximated as the optimal frequency. The objective of this section is to explore the possibility of thermal ablation and to investigate the effects of ultrasound exposure time on the thermal ablation for DPLUS with such a long thin waveguide. Before measuring the temperature rise in the tissue and conducting the thermal ablation experiments, a sequence of experiments was conducted for determining the transmitted axial vibration velocity amplitude v_{max} right after the contact interface between the tissue and thin waveguide tip. Such preparations are necessary since the transmitted axial vibration velocity determines the acoustic field, ultrasound power deposition field, and temperature distribution in the tissue, thus giving a quantitative understanding of the axial vibration velocity amplitude v_{max} required for realizing thermal ablation. Here, we determined using v_{max} of 1 m/s. Maximum v_{max} that might be realized by this DPLUS prototype is ~1.4 m/s.

A. MEASUREMENT OF THE VIBRATION ATTENUATION IN THE THIN WAVEGUIDE

The fabricated DPLUS had a 1-m long fused quartz thin waveguide. The vibration velocity at the longitudinal direction of the thin waveguide tip center ($r = 0$) was measured using a Laser Doppler Vibrometer (LDV, LV-1800, ONO SOKKI, Co., Ltd., Yokohama, Japan) as illustrated in Fig. 5. By gradually cutting the thin waveguide from 1 m long to 0.7 m long, and finally to 0.5 m long, the tip vibration velocity was measured. The results are shown in Fig. 5. In these measurements, DPLUS was driven under 50 burst cycles, 1.019 MHz, and 30 V_{p-p}. Under 1.019 MHz, the axial vibration at the thin waveguide tip (from $r = 0$ to $r = a$) behaves like a piston movement which could increase the accuracy for the vibration attenuation measurement since off-center ($r \approx 0$) measurement has small effect on the vibration velocity values. In addition, low-frequency (1.019 MHz) and relatively narrow-band (50 burst cycles) measurements reduce the wave dispersion effect in the thin waveguide. 50 burst cycles were not long enough for exciting the resonance in the thin waveguide studied here. By the frequency and burst cycle settings, the effect of wave dispersion was assumed negligible and therefore the attenuation of the measured vibration velocity only comes from the material damping. From the change of maximum vibration velocity amplitude at different thin waveguide lengths as shown in Fig. 5, the vibration amplitude attenuation coefficient α_{tw} was calculated using Eq. (1), which results in 0.011 dB/MHz/cm (calculated from 0.7 m to 1 m) and 0.0136 dB/MHz/cm (calculated from 0.5 m to 1 m). The vibration amplitude attenuation coefficient α_{tw} becomes ~0.0123±0.0013 dB/MHz/cm, which is almost 1/10 of Nitinol material (~0.11 dB/MHz/cm) that was measured before [18]. Our measurements at 3.427 MHz showed similar value ~0.1 dB/MHz/cm, and therefore the measured α_{tw} might be effective at least within 3.427 MHz.

Under the vibration amplitude attenuation coefficient α_{tw} of ~0.0123±0.0013 dB/MHz/cm, modeling results in Fig. 4 indicate that the optimal frequency is at 2.15 MHz under the thin waveguide radius of 0.6 mm. The working frequency of DPLUS was designed as 2.2 MHz which is close enough to the optimal frequency. In the later experiments, DPLUS with a 0.5 m long fused quartz thin waveguide was used.

B. AXIAL VIBRATION VELOCITY SHAPE OF THE EXCITED WAVE

The axial vibration velocity shape of the excited wave under 2.2 MHz is shown in Fig. 6. The transient vibration velocity at the longitudinal direction of the thin waveguide tip with the radial distance r varying from 0 to a (=0.6 mm) was measured using the LDV. The measured vibration velocity distribution from $r = 0$ to $r = a$ at the same transient time represents the axial vibration velocity shape. DPLUS was driven under 2.2 MHz and 10 V_{p-p}. The measurements were conducted at four radial directions as illustrated in

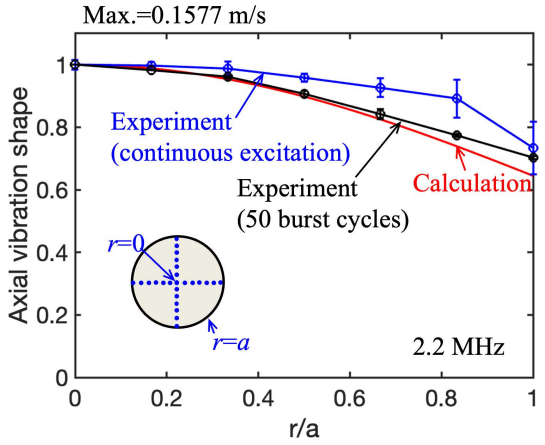

FIGURE 6. Axial vibration velocity shape at 2.2 MHz. Results were normalized to the maximum value given above the figure.

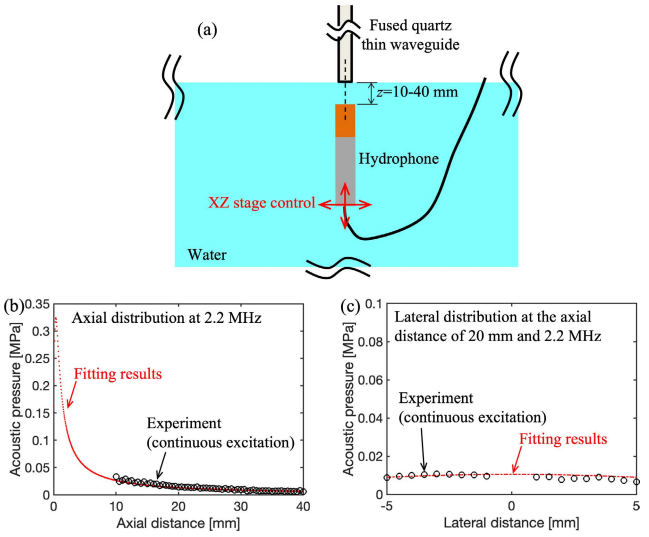

FIGURE 7. Acoustic pressure distributions at 2.2 MHz. (a) Illustration of the measurement setup. (b) Axial acoustic pressure distribution. (c) Lateral acoustic pressure distribution at the axial distance of 20 mm.

Fig. 6, and the results are shown by the averaged vibration velocity at each radial distance r with an error bar. Calculation was obtained by solving Eq. (S2) in the supplementary material. It can be observed that the experimental results of 50 burst cycles have excellent agreement with the calculation. Under continuous excitation, however, certain difference occurs although the overall tendency is close to the calculation. This might be caused by the excitation of the L(0,1) mode and the first flexural mode. The flexural mode might result from the alignment error between the axis-symmetric axis of the thin waveguide and the axis-symmetric axis of the parabolic-reflectors structure during the gluing process. The axial vibration velocity shape measured under 50 burst cycles was confirmed axially symmetric but that of continuous excitation was slightly different from axially symmetric (with the maximum difference in the measured axial vibration velocity at four radial directions of 16 % at $r = 0.8a$). However, in the lateral acoustic pressure measurement in Fig. 7(c), we could confirm the symmetric distribution relative to the center axis, and therefore it was assumed that the flexural mode was excited with relatively small vibration amplitude and the effect of which was not a large concern.

C. TRANSMITTED VIBRATION VELOCITY AFTER THE CONTACT INTERFACE BETWEEN THE TISSUE AND THIN WAVEGUIDE

Since the transmitted axial vibration velocity v from the thin waveguide to the tissue is not directly measurable, we replaced tissue with water and estimated the transmitted axial vibration velocity from the thin waveguide to water. This estimated vibration velocity was assumed equal to the transmitted axial vibration velocity v from the thin waveguide to tissue. The estimation is based on the acoustic pressure measurement in water.

Figure 7(a) illustrates the setup for the acoustic pressure measurement. The 0.5 m long fused quartz thin waveguide of DPLUS was vertically immersed in water with the immersion depth ∼0.3 mm. The water tank is cubic with the width of ∼300 mm, and sponges were attached to its walls for avoiding ultrasound reflections. A needle hydrophone (HNR 0500, Onda Corporation, California, USA) was coaxially aligned for measuring the acoustic pressure. The axial distance is denoted as z as shown in Fig. 7(a). The axial acoustic pressure distribution was measured from the axial distance z of 10 to 40 mm; the lateral acoustic pressure distribution was measured at the lateral distance from -5 to 5 mm and the axial distance of 20 mm. The measurement step was 0.5 mm. These axial and lateral distance setups were determined for avoiding the wave interference between the emitted wave from the thin waveguide tip (ϕ1.2mm) and the reflected wave from the hydrophone tip (ϕ2.5mm). Since their tip diameters are relatively large, wave interference such as standing wave generation could totally change the measured acoustic pressure distribution at close axial distance such as below 10 mm. XYZ stages (OSMS20-35(XY) and OSMS80-20ZF-0B, SIGMAKOKI Co., Ltd., Tokyo, Japan) and a stage controller (SHOT-304GS, SIGMAKOKI Co., Ltd., Tokyo, Japan) were used for controlling the positioning of the hydrophone. The stage controller was connected to a personal computer via GPIB. Communications to the stages were programmed. DPLUS was driven continuously under 2.2 MHz and 10 V_{p-p}.

Results are shown in Figs. 7(b)-(c). Fitting results were obtained by solving $P(Z, X)$ of Eq. (S3) at the frequency of 2.2 MHz. From the fitting results, the transmitted vibration velocity amplitude v_{max} right after the contact interface between water and thin waveguide tip (simplified as v_{max} in water) under 10 V_{p-p} applied voltage is 0.13 m/s. Under the same applied voltage to DPLUS, the measured vibration velocity amplitude $v_{max-air}$ right after the contact interface

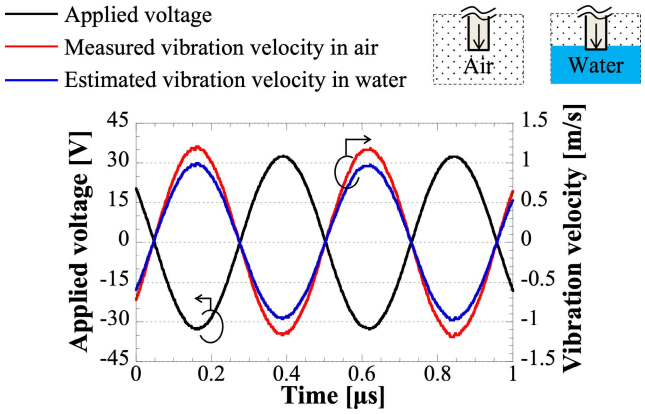

FIGURE 8. Applied voltage and vibration velocity at the thin waveguide tip for realizing the vibration velocity amplitude v_{max} in water of 1 m/s.

between air and thin waveguide tip (simplified as $v_{max-air}$ in air) by the LDV is 0.1577 m/s. The ratio of v_{max} and $v_{max-air}$ in air is 82.4%. To realize v_{max} in water of 1 m/s, $v_{max-air}$ in air was calculated by dividing $v_{max} = 1$ m/s by the ratio 82.4%, which becomes 1.213 m/s. The measured transient vibration velocity (at $r = 0$) under $v_{max-air}$ in air of 1.213 m/s is shown by the red curve in Fig. 8. The blue curve represents the estimated vibration velocity in water at v_{max} in water of 1 m/s, which was calculated as the product of the red curve and the ratio 82.4%. The required voltage for realizing these vibration velocities is shown by the black curve, and the peak-to-peak voltage is 65.5 V_{p-p}.

D. TEMPERATURE MEASUREMENT IN THE TISSUE AND THERMAL ABLATION EXPERIMENTS

After determining the applied voltage to DPLUS (65.5 V_{p-p}), the temperature measurement in the tissue and thermal ablation experiments were conducted. Under different ultrasound exposure time, the tissue temperature rise was measured; if lesion occurs, the size of the ablated tissue was measured using a caliper after the temperature rise measurement. Here, we demonstrate under the ultrasound exposure time of 1 s, 5 s, 10 s, and 20 s. DPLUS was driven continuously for reaching these exposure time.

Figure 9 illustrates the measurement setup. Fresh chicken breast tissue was purchased from a local supermarket. Four samples were prepared, each with the size of ~4 cm×3 cm×3 cm. Each sample was used for the experiment under one ultrasound exposure time. Each sample was sliced along the length direction resulting in the half sample height of 1.5 cm as illustrated in Fig. 9(b). Before the measurement, four samples were degassed and relaxed for 2 hours at the room temperature (24 °C). The measurement procedure is explained as follows. A half-sliced sample was placed on a stage as shown in Fig. 9(a). Then a K-type thin film thermocouple (GMT-TC-SB7.5, GEOMATEC Co., Ltd., Yokohama, Japan) was attached to the top (flat) surface of the half-sliced sample with the distance from the thermocouple joint to the tissue edge of ~1 mm. The polyimide film

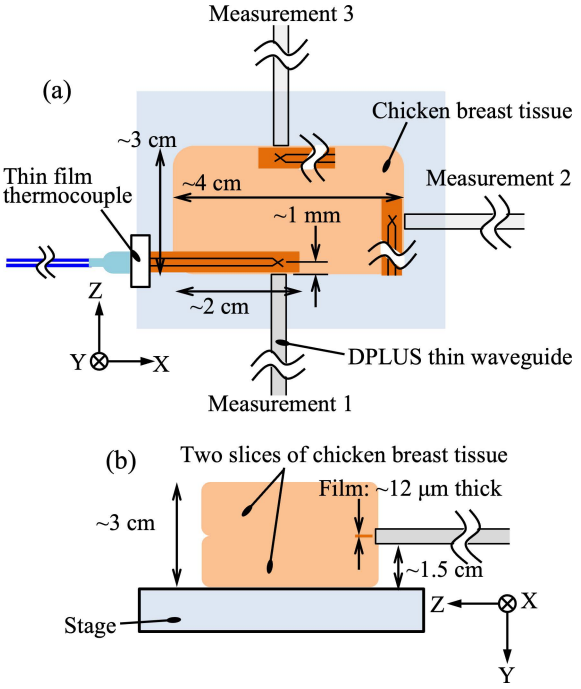

FIGURE 9. Setup for the temperature measurement and thermal ablation experiments. (a) Top and (b) side view.

thickness of the thermocouple is ~12 μm, and the measurement artefacts such as viscous heating from this thermocouple can be minimized. The thickness of the thermocouple was in the Y direction which is to minimize the disturbance of the acoustic field. The second-half sample was then placed on top of the first half and totally covered the thermocouple as shown in Fig. 9(b). The tissue was pressed for reducing the air bubble possibly trapped at the interface of two half-sliced samples. Next, the position of DPLUS was manually controlled by precision stages for aligning the axis-symmetric axis of the thin waveguide to the interface of two half-sliced tissue. DPLUS was then driven under 65.5 V_{p-p} and 2.2 MHz for one ultrasound exposure time. When the ultrasound exposure time is 1 s or 5 s such that tissue ablation does not occur, the temperature rise was measured 5 times at one measurement location; if tissue ablation occurs, the temperature rise was measured once at one measurement location. For measuring the temperature rise at different locations, the tissue sample was rotated in the X-Z plane with the thermocouple realigned, and typically three locations were measured as indicated by "Measurement 1" to "Measurement 3" in Fig. 9 (a). The temperature was recorded by a temperature data logger (GL200 midi LOGGER, GRAPHTEC Co., Ltd., Yokohama, Japan), with the sampling time of 0.1 s.

For predicting the tissue temperature rise, transient temperature simulations using a commercial Finite-Element-Analysis software Femtet (Murata Software Co., Ltd., Yokohama, Japan) were conducted. The simulation model is shown in Fig. S1, with the tissue material properties listed in TABLE 1. The only change is the acoustic absorption

coefficient α_{ts} which was measured by comparing the relative amplitude of ultrasound through transmission measurements in the tissue sample and in free water [26]. For this measurement, a 1 MHz transducer with a diameter of 20 mm was used as a transmitter and a hydrophone (HNR 0500, Onda Corporation, California, USA) was used as a receiver. The measurement of a 10.725±0.637 mm thick chicken breast tissue sample taken from the same source sample for the temperature measurement showed the acoustic attenuation coefficient of 1.154±0.185 dB/MHz/cm. Assume an absorption to scattering ratio of 73/27 based on canine muscle attenuation at 37 °C [27], the acoustic absorption coefficient was estimated as 0.843±0.135 dB/MHz/cm. The acoustic absorption coefficient of 0.84 dB/MHz/cm was used in the simulation. The ultrasound power deposition fields were calculated by MATLAB and then imported to Femtet for the transient temperature simulation.

The temperature rise results are shown in Fig. 10. The temperature baseline is 24 °C. Experimental results were analyzed from the measurements at typically three locations and were plotted as the black curves. For the simulation results, the maximum temperature rise in the tissue is shown by the blue curve, which occurs at the lateral distance of 0 mm and axial distance of 0.45 mm, 0.48 mm, 0.55 mm, and 0.55 mm for 1 s, 5 s, 10 s, and 20 s, respectively. For considering the possible positioning error of the thermocouple, the temperature rises at the lateral distance of 0 mm and axial distance of 0.8 mm, 1 mm, and 1.2 mm were plotted in Fig. 10 under each ultrasound exposure time. The experimental results under 1 s ultrasound exposure (Fig. 10(a)) have excellent agreement with the simulation results. For 5 s and 10 s ultrasound exposure (Figs. 10(b)-10(c)), the experimental temperature rises are within the simulation results, but certain difference could be clearly observed especially after the ultrasound is off. In addition, the temperature rises for the 5 s exposure showed the saturation tendency which does not occur in the simulation. For 20 s ultrasound exposure (Fig. 10(d)), temperature rise curves under four exposure trials are shown. The temperature rise curves below 5 s had excellent agreement with the simulation results, but then showed abrupt change. The possible reasons for the differences occurred under 5 s, 10 s, and 20 s exposure are explained as follows. First, the thermal properties (such as thermal conductivity and thermal diffusivity) of the chicken breast tissue were not measured which could be different from the values used in the simulation (TABLE 1). Such difference could possibly explain the different tendencies when the ultrasound is off. Second, the acoustic properties such as attenuation and absorption coefficients of the tissue are functions of temperature and thermal dose [27], however, such dynamics were not simulated which could possibly explain the difference in the temperature rise and fall curves. Third, as shown in the axial vibration velocity shape in Fig. 6, the experimental results under continuous excitation had certain difference with the calculation, which might result in accumulated error for the simulated temperature field. Fourth, the fused quartz thin waveguide was glued to the DPLUS parabolic-reflectors structure using epoxy, the temperature measurement at the epoxy surface showed over 100 °C within 1 s and long-time driving of DPLUS could possibly result in connection failure and abrupt change of the connection stability. This could explain the abrupt change of the temperature curves under 20 s exposure. Fifth, temperature rise in the PZT results in the resonant frequency shift, which requires precise and fast resonant frequency control system. Sixth, under the ultrasound radiation force, the tissue near the interface between two half-sliced sample might displace relative to each other which results in the abrupt change in the measured temperature curves. These factors are mixed, and to understand the effect of each factor requires further in-depth studies.

The relation between the lesion size and the ultrasound exposure time is shown in Fig. 11. Fig. 11(a) shows the lesion

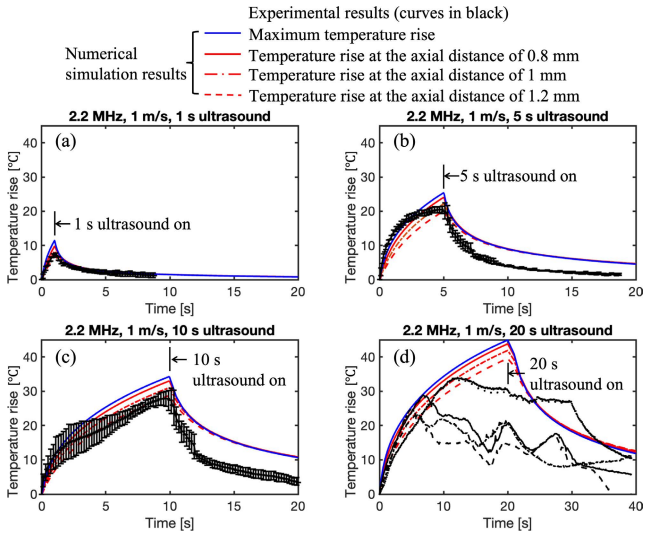

FIGURE 10. Temperature rises measurement under (a) 1 s, (b) 5 s, (c) 10 s, and (d) 20 s of ultrasound exposure.

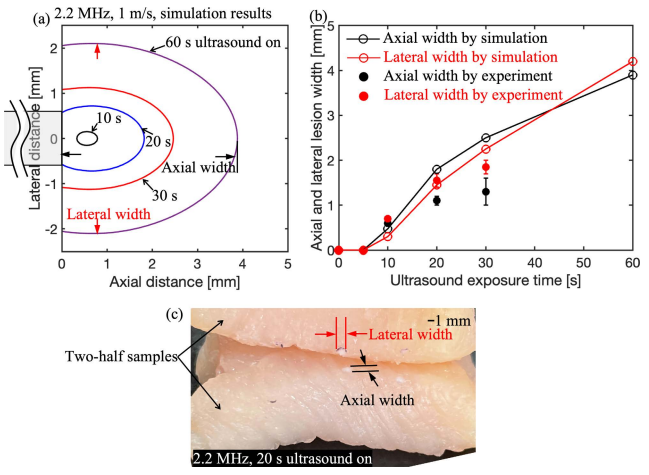

FIGURE 11. Thermal ablation experiments. (a) Simulated lesion size. (b) Ablated tissue size against ultrasound exposure time. (c) Illustration of the lesion size measurement in the experiment.

size estimated by thermal dose, which was calculated as the equivalent minutes at the reference temperature (43 °C) [28]:

$$\mathrm{TD} = \sum_{t=0}^{t_{\mathrm{end}}} R^{43-T}\,\Delta t, \quad \begin{cases} R = 0, & T < 39^{\circ}\mathrm{C} \\ R = 0.25, & 39^{\circ}\mathrm{C} \le T \le 43^{\circ}\mathrm{C} \\ R = 0.5, & T > 43^{\circ}\mathrm{C} \end{cases}, \tag{3}$$

where Δt is the time step, T is the temperature at time t. Here, a conservative approach was adopted which assumes TD $\geq$ 300 mins for total necrosis. The estimated lesion has an elliptical shape and the size increases with exposure time. The DPLUS thin waveguide is aligned along the lateral direction in Fig. 11(a). The axial width is defined as the distance from the interface of thin waveguide and tissue to the maximum axial distance of the lesion; the lateral width is defined as the maximum lateral distance of the lesion. The plot of axial and lateral width against the ultrasound exposure time is shown in Fig. 11(b). Experimental results were analyzed under three measurement locations. The axial width and lateral width both increase with the ultrasound exposure time. Below the ultrasound exposure time of 20 s, experimental results are close to the simulation results. The measured lateral width of the lesion increased from 0.6 mm to 1.1 mm, and to 1.3 mm for 10 s, 20 s, and 30 s, respectively. The maximum axial and lateral width in the experiments are smaller than 2 mm. From the simulation results, the axial width is slightly larger than the lateral width below the ultrasound exposure time of 30 s, but it is opposite in the experiments. In addition, the measured axial width and lateral width increases slowly under the exposure time of 30 s compared with simulation. Such differences between experiments and simulation might be again explained by the listed reasons for the temperature rise results.

E. DISCUSSIONS

For the proposed theoretical model of DPLUS for thermal treatments, we considered the ultrasound reflection and transmission at the contact interface between the tissue and thin waveguide. If the resonance excitations in the thin waveguide and tissue are not considered, there is a large acoustic impedance mismatch ($\sim$13 MRayls for thin waveguide and $\sim$1.5 MRayls for tissue) and the ultrasound transmission to the tissue is not efficient. To realize optimal power transmission, acoustic impedance matching layer can be designed. Considering the optimal power transmission at each frequency in the modeling, the optimal frequency would depend on the vibration attenuation in the thin waveguide and the vibration shape in the matching layer material, which might change from the current modeling results. To conduct such modeling also requires the consideration of the dispersion nature of the PC waves in both the thin waveguide and matching layer. In addition, for inducing better thermal effects to the tissue, we usually prefer continuous-wave excitation of DPLUS such that the temporal average acoustic intensity I_{ta} can be maximized by neglecting the duty ratio of the driving signal. Continuous-wave excitation of DPLUS means DPLUS is driven at resonance as the case in the experiments. Under resonance, the acoustic impedance can be roughly written as $\rho c/Q$ where ρ is the material density, c is the sound velocity, and Q is the mechanical quality factor. This resonant acoustic impedance can be relatively close to the acoustic impedance of tissue ($\sim$1.5 MRayls) and therefore acoustic impedance matching (layer) is not necessary. Considering the above discussions, acoustic impedance matching layer was not modeled in the proposed model.

The modeling results in Fig. 4 show the frequency dependence of the maximum steady-state temperature in the tissue under the constant incident vibration velocity amplitude $v_{\mathrm{in-max}}$ and the variation of vibration attenuation coefficient α_{tw} from 0.01 to 0.02 dB/MHz/cm. The effectiveness of the modeling methods for the acoustic and temperature fields had been verified by our earlier work [19]. Therefore, in this paper, we did not show the experimental verification of the frequency dependence, instead, we presented new modeling results which added the effects of the vibration attenuation in the thin waveguide, and we verified the temperature rise in the tissue at the optimal working frequency and different ultrasound exposure time.

From the measured axial vibration velocity shape under continuous excitation in Fig. 6, flexural mode might be excited although the vibration amplitude might be small. To eliminate the flexural mode, the assembling process of DPLUS needs to be improved. The axis-symmetric axis of the thin waveguide and the axis-symmetric axis of the parabolic-reflectors structure must be aligned properly.

Based on the speculated reasons for the difference of temperature rise curves between simulation and experiments in Fig. 10, the following in-depth studies might be important. First, to study thermal ablation in the tissue-like materials with known acoustic and thermal properties such as gel phantom. Second, to improve the vibration stability of the thin waveguide. For example, the stress in the thin waveguide might reach $\sim$13 MPa under the vibration velocity amplitude of 1 m/s, and epoxy with the bonding strength much higher than 13 MPa is required for avoiding the bonding failure during long-time operation of DPLUS. Third, to develop the measurement system that can monitor the tissue temperature and tissue ablation in real time without the insertion of thermocouple and slice of tissue sample, such as acoustic radiation force ultrasound imaging, magnetic resonance imaging.

Within the ultrasound exposure time of 20 s, the measured axial and lateral width of the lesion are smaller than 2 mm, which are smaller than one HIFU exposure ($<\sim$5 s, 3 mm in the lateral direction and 12 mm in the axial direction) and common interstitial ultrasound applicators (in the order of mins, in the order of 1 cm). This indicate that the developed DPLUS technique is for the treatments of small-size tumor. In terms of the required time for one exposure, DPLUS is comparable to HIFU, and similarly, multiple exposures are required for ablating relatively large-size tumor. Since the DPLUS delivers ultrasound from the thin waveguide tip, the

target tumor must physically contact with the thin waveguide tip otherwise it might be difficult to treat. However, due to the small diameter of the DPLUS thin waveguide, the risk of complications for practical treatments might be small.

The presented thermal ablation experiments showed that for thermal ablation was achieved by a long thin-waveguide DPLUS. This is an important research progress compared with our earlier work [19]. In-depth studies are required for understanding the role of DPLUS in the field of MIT based thermal ablation.

V. CONCLUSION

In this paper, based on the proposed theoretical model of DPLUS for thermal treatments, DPLUS with a 0.6-mm radius and 1-m long fused quartz thin waveguide working at the optimal frequency of 2.2 MHz was fabricated and the thermal effects to the tissue under different ultrasound exposure time were studied. Since the transmitted axial vibration velocity amplitude $v_{\max}$ (at $r = 0$) right after the contact interface between the tissue and thin waveguide cannot be measured directly, it was estimated based on the acoustic pressure measurement in water and the curve fitting by solving the Rayleigh-Sommerfeld integral. Under the transmitted axial vibration velocity amplitude $v_{\max}$ of 1 m/s and the ultrasound exposure time of 1 s, 5 s, 10 s, 20 s, the temperature rise curves showed overall good agreements between the simulation and experiments. The possible reasons for the differences were listed. To investigate the reasons, further in-depth studies are required. Under the axial vibration velocity amplitude $v_{\max}$ of 1 m/s and the ultrasound exposure time of 10 s, 20 s, and 30 s, lesion was observed in the tissue. The lesion size increases with exposure time, and the measured axial and lateral width of the lesions are smaller than 2 mm. Using the data at 10 s ultrasound exposure, the increase of lateral lesion width (in mm) per vibration velocity (in m/s) per ultrasound exposure (in s) is roughly estimated as 0.06. The presented results in this paper showed that for thermal ablation was achieved by a long thin-waveguide DPLUS which becomes an important progress of DPLUS towards practical MIT applications.

REFERENCES

[1] U. Rosenschein, J. J. Bernstein, E. DiSegni, E. Kaplinsky, J. Bernheim, and L. A. Rozenzsajn, "Experimental ultrasonic angioplasty: Disruption of atherosclerotic plaques and thrombi in vitro and arterial recanalization in vivo," *J. Amer. College Cardiol.*, vol. 15, no. 3, pp. 711–717, Mar. 1990.

[2] B. J. O'Daly, E. Morris, G. P. Gavin, J. M. O'Byrne, and G. B. McGuinness, "High-power low-frequency ultrasound: A review of tissue dissection and ablation in medicine and surgery," *J. Mater. Process. Technol.*, vol. 200, nos. 1–3, pp. 38–58, May 2008.

[3] G. P. Gavin, G. B. McGuinness, F. Dolan, and M. S. J. Hashmi, "Performance characteristics of a therapeutic ultrasound wire waveguide apparatus," *Int. J. Mech. Sci.*, vol. 49, no. 3, pp. 298–305, Mar. 2007.

[4] G. P. Gavin, "Experimental and numerical investigation of therapeutic ultrasound angioplasty," Ph.D. dissertation, School Mech. Manuf. Eng., Dublin City Univ., Dublin, Ireland, 2005.

[5] T. Irie, N. Tagawa, M. Tanabe, T. Moriya, M. Yoshizawa, T. Iijima, K. Itoh, T. Yokoyama, H. Kumagai, and N. Taniguchi, "Transmission of 100-MHz-range ultrasound through a fused quartz fiber," *J. Med. Ultrason.*, vol. 38, no. 3, pp. 119–127, Apr. 2011.

[6] T. Moriya, Z. Hu, and Y. Tanahashi, "Development of flexible acoustic transmission line for intravascular ultrasonography," in *Proc. IEEE Ultrason. Symposium. Int. Symp.*, Oct. 2000, pp. 1227–1230.

[7] T. Irie, M. Sato, N. Tagawa, M. Yoshizawa, and T. Moriya, "A study for real-time B-mode imaging using 100-MHz-range ultrasound through a fused quartz fiber," in *Proc. IEEE Int. Ultrason. Symp. (IUS)*, Sep. 2017, pp. 1–4.

[8] T. Irie, T. Hasegawa, K. Itoh, N. Hirota, N. Tagawa, M. Yoshizawa, T. Moriya, and T. Iijima, "Tissue imaging using the transmission of 100-MHz-range ultrasound through a fused quartz fiber," in *Proc. IEEE Int. Ultrason. Symp. (IUS)*, Jul. 2013, pp. 2010–2013.

[9] P. D. Tyréus, W. H. Nau, and C. J. Diederich, "Effect of applicator diameter on lesion size from high temperature interstitial ultrasound thermal therapy," *Med. Phys.*, vol. 30, no. 7, pp. 1855–1863, Jun. 2003.

[10] T. Moriya, N. Tagawa, Y. Tanabashi, Y. Takamura, and S. Yagi, "Thermal therapy using flexible fibers as transmission line (SoFT)," in *Proc. IEEE Symp. Ultrason.*, Oct. 2003, pp. 1463–1466.

[11] B. J. Jarosz and S. S. James, "Integrated temperature sensor for determination of ultrasound interstitial applicator heating effects," *IEEE Trans. Instrum. Meas.*, vol. 54, no. 3, pp. 1171–1174, Jun. 2005.

[12] T. Moriya, Z. Hu, Y. Tanahashi, and Y. Seki, "Development of an ultrasonic applicator for SonoFiber therapy: A thermal therapy using fused-quartz fibers (SoFT)," *Jpn. J. Appl. Phys.*, vol. 42, no. 1, pp. 3262–3264, May 2003.

[13] D. Atkinson and G. Hayward, "The generation and detection of longitudinal guided waves in thin fibers using a conical transformer," *IEEE Trans. Ultrason., Ferroelectr., Freq. Control*, vol. 48, no. 4, pp. 1046–1053, Jul. 2001.

[14] D. Atkinson and G. Hayward, "Fibre waveguide transducers for Lamb wave NDE," *IEE Proc.-Sci., Meas. Technol.*, vol. 145, no. 5, pp. 260–268, Sep. 1998.

[15] K. Chen, T. Irie, T. Iijima, T. Kasashima, K. Yokoyama, S. Miyake, and T. Morita, "Hard-type piezoelectric materials based double-parabolic-reflectors ultrasonic transducer (DPLUS) for high-power ultrasound," *IEEE Access*, vol. 10, pp. 26117–26126, 2022.

[16] K. Chen, T. Irie, T. Iijima, and T. Morita, "Wideband multi-modes excitation by one double-parabolic-reflectors ultrasonic transducer (DPLUS)," *IEEE Trans. Ultrason. Ferroelectr., Freq. Control*, vol. 67, no. 8, pp. 1620–1631, Aug. 2020.

[17] K. Chen, T. Irie, T. Iijima, T. Kasashima, K. Yokoyama, and T. Morita, "Selection criteria of piezoelectric materials for double-parabolic-reflectors ultrasonic transducers (DPLUS) for high-power ultrasound," *Jpn. J. Appl. Phys.*, vol. 60, no. 10, Sep. 2021, Art. no. 106504.

[18] K. Chen, T. Irie, T. Iijima, and T. Morita, "Double-parabolic-reflectors ultrasonic transducer with flexible waveguide for minimally invasive treatment," *IEEE Trans. Biomed. Eng.*, vol. 68, no. 10, pp. 2965–2973, Oct. 2021.

[19] K. Chen, T. Irie, T. Iijima, S. Miyake, and T. Morita, "Optimization of the thin waveguide for double-parabolic-reflectors ultrasonic transducers (DPLUS) for thermal ablation," *IEEE Trans. Biomed. Eng.*, early access, Aug. 8, 2022, doi: 10.1109/TBME.2022.3197213.

[20] Y. Kim, G. A. Parada, S. Liu, and X. Zhao, "Ferromagnetic soft continuum robots," *Sci. Robot.*, vol. 4, no. 33, Aug. 2019, Art. no. eaax7329.

[21] C. H. Sherman and J. L. Butler, *Transducers and Arrays for Underwater Sound*. New York, NY, USA: Springer, 2007, pp. 438–501.

[22] M. Redwood, *Mechanical Waveguides: The Propagation of Acoustic and Ultrasonic Waves in Fluids and Solids with Boundaries*, New York, NY, USA: Pergamon, 1960, pp. 32–35 and 135–137.

[23] H. H. Pennes, "Analysis of tissue and arterial blood temperatures in the resting human forearm," *J. Appl. Physiol.*, vol. 85, no. 1, pp. 5–34, Jul. 1998.

[24] J. C. Chato, D. P. Keith, and B. R. Robert, *Thermal Dosimetry and Treatment Planning*. Cham, Switzerland: Springer, 2012, pp. 36–49.

[25] K. Ono, "A comprehensive report on ultrasonic attenuation of engineering materials, including metals, ceramics, polymers, fiber-reinforced composites, wood, and rocks," *Appl. Sci.*, vol. 10, no. 7, p. 2230, Mar. 2020.

[26] T. Tiennot, H. A. S. Kamimura, S. A. Lee, C. Aurup, and E. E. Konofagou, "Numerical modeling of ultrasound heating for the correction of viscous heating artifacts in soft tissue temperature measurements," *Appl. Phys. Lett.*, vol. 114, no. 20, May 2019, Art. no. 203702.

[27] C. A. Damianou, N. T. Sanghvi, F. J. Fry, and R. Maass-Moreno, "Dependence of ultrasonic attenuation and absorption in dog soft tissues on temperature and thermal dose," *J. Acoust. Soc. Amer.*, vol. 102, no. 1, pp. 628–634, Jul. 1997.
[28] S. A. Sapareto, "Thermal dose determination in cancer therapy," *Int. J. Radiat. Oncol. Biol. Phys.*, vol. 10, no. 6, pp. 787–800, Apr. 1984.

KANG CHEN was born in Zhejiang, China, in 1994. He received the B.E. degree from Zhejiang Normal University, China, in 2017, and the M.S. degree from the Graduate School of Frontier Sciences, The University of Tokyo, Japan, in 2020, where he is currently pursuing the Ph.D. degree.

He was worked as a Research Assistant at The Chinese University of Hong Kong and City University of Hong Kong, in 2017. His research interest includes ultrasonic transducers for biomedical applications.

TAKASUKE IRIE (Member, IEEE) received the B.E. degree from the Department of Electronics and Communication Engineering, Musashi Institute of Technology, in 1968, and the Dr.Eng. degree from the Graduate School of System Design, Tokyo Metropolitan University, in 2011.

He worked at Aloka Company Ltd., from 1968 to 1993, and Acuson Nippon Company Ltd., from 1993 to 2000. Since 2000, he has been working at Microsonic Company Ltd. He is currently the CEO of the company and also the Guest Professor of Tokyo Metropolitan University. His research interests include puncture-needle type ultrasonic transducer and ultrasonic microscope.

TAKASHI IIJIMA received the B.Eng., M.Eng., and Dr.Eng. degrees in material science from Tohoku University, in 1983, 1985, and 1988, respectively. He worked at YAMAHA Corporation, from 1988 to 1993. From 1993 to 2020, he worked at the National Institute of Advanced Industrial Science and Technology (AIST). From 2020 to 2022, he was a Contract Professor at the Tokyo University of Science. He is currently an Invited Senior Researcher of the Global Zero Emission Research Center, AIST, and a Guest Professor at the Tokyo University of Science.

His research interests include ferroelectric thin films, piezo MEMS, ultrasonic transducers, and hydrogen embrittlement.

SUSUMU MIYAKE received the B.S., M.S., and Ph.D. degrees from The University of Tokyo, in 2016, 2018, and 2021, respectively.

He became an Assistant Professor at the Graduate School of Frontier Sciences, The University of Tokyo, in 2021. His current research interests include the high-power characteristics of piezoelectric materials and lead-free piezoelectric materials.

TAKESHI MORITA (Member, IEEE) received the B.Eng., M. Eng., and Dr.Eng. degrees in precision machinery engineering from The University of Tokyo, in 1994, 1996, and 1999, respectively.

After being a Postdoctoral Researcher at the RIKEN (the Institute of Physical and Chemical Research) and at EPFL (Swiss Federal Institute of Technology), he became a Research Associate at Tohoku University, in 2002. He was an Associate Professor at The University of Tokyo, in 2005. He has been a Full Professor, since 2018. His research interests include piezoelectric actuators and sensors, their fabrication processes and control systems.